JBC RESEARCH ARTICLE

Transcriptional coregulator Ess2 controls survival of post-thymic CD4$^+$ T cells through the Myc and IL-7 signaling pathways

Received for publication, December 29, 2021, and in revised form, July 18, 2022 Published, Papers in Press, August 3, 2022,
https://doi.org/10.1016/j.jbc.2022.102342

Ichiro Takada[1,*,‡], Shinya Hidano[2,‡], Sayuri Takahashi[3,‡], Kaori Yanaka[4], Hidesato Ogawa[5], Megumi Tsuchiya[5], Atsushi Yokoyama[6], Shingo Sato[7], Hiroki Ochi[8], Tohru Nakagawa[9], Takashi Kobayashi[2], Shinichi Nakagawa[10], and Makoto Makishima[1,*]

From the [1]Division of Biochemistry, Department of Biomedical Sciences, School of Medicine, Nihon University, Itabashi-ku, Tokyo, Japan; [2]Department of Infectious Diseases Control, Faculty of Medicine, Oita University, Oita, Japan; [3]Department of Urology, The University of Tokyo, Bunkyo-ku, Tokyo, Japan; [4]RNA Biology Laboratory, RIKEN Advanced Research Institute, Wako, Saitama, Japan; [5]Graduate School of Frontier Biosciences, Osaka University, Suita, Japan; [6]Department of Molecular Endocrinology, Tohoku University Graduate School of Medicine, Sendai, Miyagi, Japan; [7]Center for Innovative Cancer Treatment, Tokyo Medical and Dental University Medical Hospital, Tokyo, Japan; [8]Department of Rehabilitation for Movement Functions, Research Institute, National Rehabilitation Center for Persons with Disabilities, Tokorozawa, Saitama, Japan; [9]Department of Urology, Teikyo University, Itabashi-ku, Tokyo, Japan; [10]RNA Biology Laboratory, Faculty of Pharmaceutical Sciences, Hokkaido University, Sapporo, Japan

Edited by Peter Cresswell

Ess2, also known as Dgcr14, is a transcriptional co-regulator of CD4$^+$ T cells. *Ess2* is located in a chromosomal region, the loss of which has been associated with 22q11.2 deletion syndrome (22q11DS), which causes heart defects, skeletal abnormalities, and immunodeficiency. However, the specific association of Ess2 with 22q11DS remains unclear. To elucidate the role of Ess2 in T-cell development, we generated *Ess2* floxed (*Ess2$^{fl/fl}$*) and CD4$^+$ T cell–specific *Ess2* KO (*Ess2$^{\Delta CD4/\Delta CD4}$*) mice using the Cre/loxP system. Interestingly, *Ess2$^{\Delta CD4/\Delta CD4}$* mice exhibited reduced naïve T-cell numbers in the spleen, while the number of thymocytes (CD4$^-$CD8$^-$, CD4$^+$CD8$^+$, CD4$^+$CD8$^-$, and CD4$^-$CD8$^+$) in the thymus remained unchanged. Furthermore, *Ess2$^{\Delta CD4/\Delta CD4}$* mice had decreased NKT cells and increased γδT cells in the thymus and spleen. A genome-wide expression analysis using RNA-seq revealed that *Ess2* deletion alters the expression of many genes in CD4 single-positive thymocytes, including genes related to the immune system and Myc target genes. In addition, Ess2 enhanced the transcriptional activity of c-Myc. Some genes identified as Ess2 targets in mice show expressional correlation with *ESS2* in human immune cells. Moreover, *Ess2$^{\Delta CD4/\Delta CD4}$* naïve CD4$^+$ T cells did not maintain survival in response to IL-7. Our results suggest that Ess2 plays a critical role in post-thymic T-cell survival through the Myc and IL-7 signaling pathways.

Transcriptional co-regulators contribute to gene expression by interacting with DNA-bound transcription factors (1). The functions of transcription co-regulators are diverse, including histone modifications, chromatin structure conversion, and chromosome structure changes. Because they regulate multiple transcription factors, transcriptional co-regulator functions *in vivo* are complex and still under investigation. We recently identified Ess2 (also known as Dgcr14 or Es2) as a transcriptional co-regulator of retinoid-related orphan nuclear receptor gamma/gamma-t (RORγ/γt) through biochemical purification and matrix-assisted laser desorption ionization–time of flight mass spectrometry analysis (2).

In humans, the *ESS2* gene was first cloned as an expression sequence tag located in the 22q11.2 locus, which is related to the 22q11.2 deletion syndrome (22q11DS; also known as DiGeorge syndrome or CATCH 22 syndrome) (3, 4). 22q11DS is a disorder caused by a small deletion, located near the middle of chromosome 22, specifically designated q11.2 (5–7). Common signs and symptoms of this syndrome include heart abnormalities, cleft palate, distinctive facial features, and schizophrenia. In addition, 22q11DS patients are often immunodeficient and experience recurrent infections, and some patients develop autoimmune disorders, including rheumatoid arthritis and Graves' disease (8). While genetically modified mouse models expressing 22q11DS phenotypes have been reported, immunodeficiency-related genes within 22q11.2 have not yet been identified.

RORγ/γt are members of the nuclear receptor superfamily, and they regulate T_H17 cell development (9, 10). Ess2 regulates *Il17a* mRNA levels, which are induced during T_H17 cell development through RORγ/γt (2). Additionally, the genes ribosomal S6 kinase 2 (Rsk2; Rps6ka3) and bromodomain adjacent to zinc finger domain 1B (Baz1b) associate with Ess2 to regulate the transcriptional activities of RORγ/γt in T_H17 cells (2). *Ess2* mRNA expression levels are higher in T_H17 cells than in naïve, T_H1, T_H2, or induced regulatory T cells (iTregs) (2). The Ess2 protein localizes in the nucleus

‡ These authors contributed equally to this work.
* For correspondence: Ichiro Takada, takada.ichiro@nihon-u.ac.jp; Makoto Makishima, makishima.makoto@nihon-u.ac.jp.

where it interacts with both transcription factors and spliceosomes (11–13). The function of Ess2 during T-cell development *in vivo* is poorly understood because homozygous *Ess2* mutant mice are embryonically lethal (14).

Our previous studies (2) suggested the possibility that Ess2 regulates T-cell development and differentiation *in vivo*. To elucidate the function of the *Ess2* gene during T-cell development *in vivo*, we generated *Ess2* gene floxed mice ($Ess2^{fl/fl}$) and CD4-specific *Ess2* knockout (KO) mice ($Ess2^{\Delta CD4/\Delta CD4}$) by crossing CD4-Cre transgenic mice (15) and $Ess2^{fl/fl}$ mice. Interestingly, these mice survive but have reduced naïve T-cell numbers. Our studies on these mice have elucidated the role of the *Ess2* gene during T-cell development.

Results

Generation of $Ess2^{\Delta CD4/\Delta CD4}$ mice

To elucidate Ess2 function *in vivo*, we generated $Ess2^{\Delta CD4/\Delta CD4}$ mice using the Cre-loxP system (Fig. S1*A*). We first generated *Ess2* KO ($Ess2^{-/-}$) and $Ess2^{+/-}$ mice by inserting a splicing acceptor into the exon 2, FRP, and loxP sequences (Fig. S1*A*). Consistent with previous reports, $Ess2^{-/-}$ mice were embryonically lethal (Fig. S1, *B* and *C*) (14). However, $Ess2^{+/-}$ mice survived and did not have any abnormal appearances or bodyweight loss (data not shown). We then crossed $Ess2^{+/-}$ mice with FLP-expressing transgenic mice (RIKEN No. RBRC01834, see Experimental procedures) to generate $Ess2^{fl/fl}$ mice (Figs. S1*A* and 1*A*).

To determine the role of Ess2 during T-cell development, we generated $Ess2^{\Delta CD4/\Delta CD4}$ by crossing $Ess2^{fl/fl}$ with CD4-Cre transgenic mice [Fig. 1*B*, (15)]. $Ess2^{fl/fl}$ littermates were used as controls. We confirmed the recombination of the *Ess2* allele in CD4 single-positive (CD4SP) and double-positive (DP) thymocytes from $Ess2^{\Delta CD4/\Delta CD4}$ mice by the detection of a 152-bp fragment (Fig. 1*B*). $Ess2^{\Delta CD4/\Delta CD4}$ mice appear normal and have a similar body weight compared to $Ess2^{fl/fl}$ mice (Fig. 1*C*). *Ess2* mRNA expression levels were significantly reduced in DP thymocytes isolated from $Ess2^{\Delta CD4/\Delta CD4}$ mice but not in double-negative (DN) thymocytes (Fig. 1*D*). These results demonstrated that the *Ess2* gene in $Ess2^{\Delta CD4/\Delta CD4}$ mice was partially deleted in DP thymocytes and completely deleted in CD4SP thymocytes.

$Ess2^{\Delta CD4/\Delta CD4}$ mice had reduced numbers of peripheral naïve T cells

We next analyzed the number of peripheral T cells in the spleens of $Ess2^{fl/fl}$ and $Ess2^{\Delta CD4/\Delta CD4}$ mice. There were no abnormalities in the spleen, and the number of splenocytes was similar in both $Ess2^{fl/fl}$ and $Ess2^{\Delta CD4/\Delta CD4}$ mice (Fig. 2*A*). However, the numbers of $CD3^+$ (Fig. 2, *B* and *C*), $CD4^+$, and $CD8^+$ T cells (Fig. 2, *D*–*F*) were all lower in the spleens of $Ess2^{\Delta CD4/\Delta CD4}$ mice compared to $Ess2^{fl/fl}$ mice. The ratios of

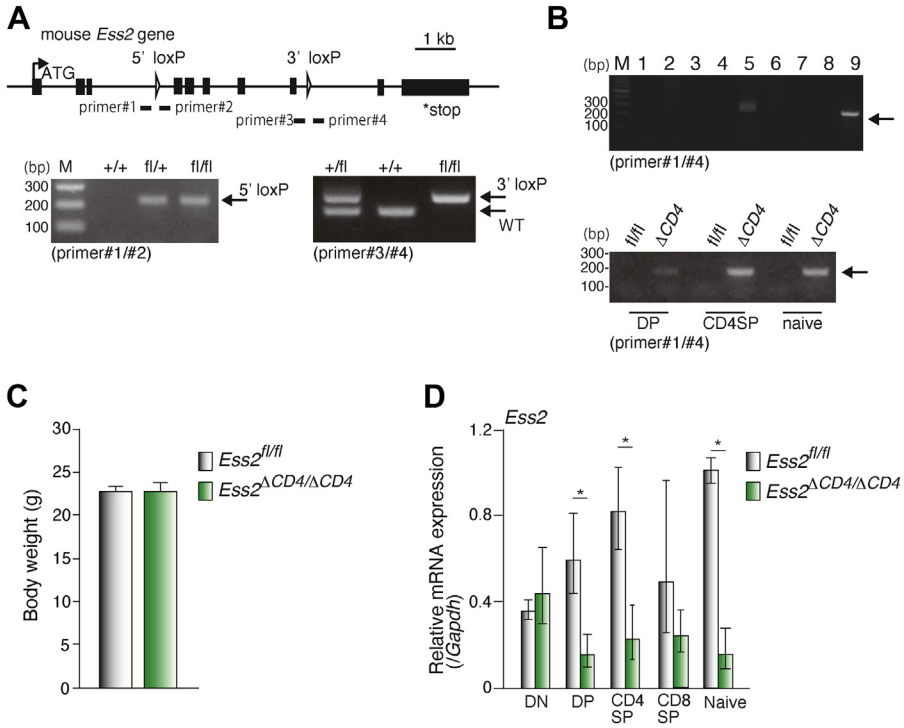

Figure 1. Generation of $Ess2^{fl/fl}$ and $Ess2^{\Delta CD4/\Delta CD4}$ mice. *A*, targeting strategy for the generation of $CD4^+$ T-cell-specific *Ess2* knockout ($Ess2^{\Delta CD4/\Delta CD4}$) mice (*upper panel*). Examples of the PCR genotyping for $Ess2^{fl/fl}$ (fl/fl), $Ess2^{fl/+}$ (fl/+), and WT (+/+) mice (*bottom panels*). *B*, *upper panel*, PCR genotyping of tissues prepared from $Ess2^{\Delta CD4/\Delta CD4}$ mice. 1; Brain, 2; Lung, 3; Heart, 4; Liver, 5; Kidney, 6; Adipose, 7; Muscle, 8; Testis, and 9; $CD4^+$ T cells; *Bottom panel*, PCR genotyping for $Ess2^{fl/fl}$ (fl/fl) and $Ess2^{\Delta CD4/\Delta CD4}$(ΔCD4) mice in $CD4^+CD8^+$ thymocytes (DP), $CD4^+CD8^-$ thymocytes (CD4SP), and naive T cells (naive). *C*, the body weights of $Ess2^{fl/fl}$ and $Ess2^{\Delta CD4/\Delta CD4}$ mice used in Figures 2 and 3. *D*, RT-qPCR of *Ess2* mRNA in thymocytes and naïve T cells normalized to the level of *Gapdh* mRNA expression. Three to four mice were used in each experiment. *p* values were calculated using Student's *t* test. $*p < 0.05$. qPCR, quantitative polymerase chain reaction.

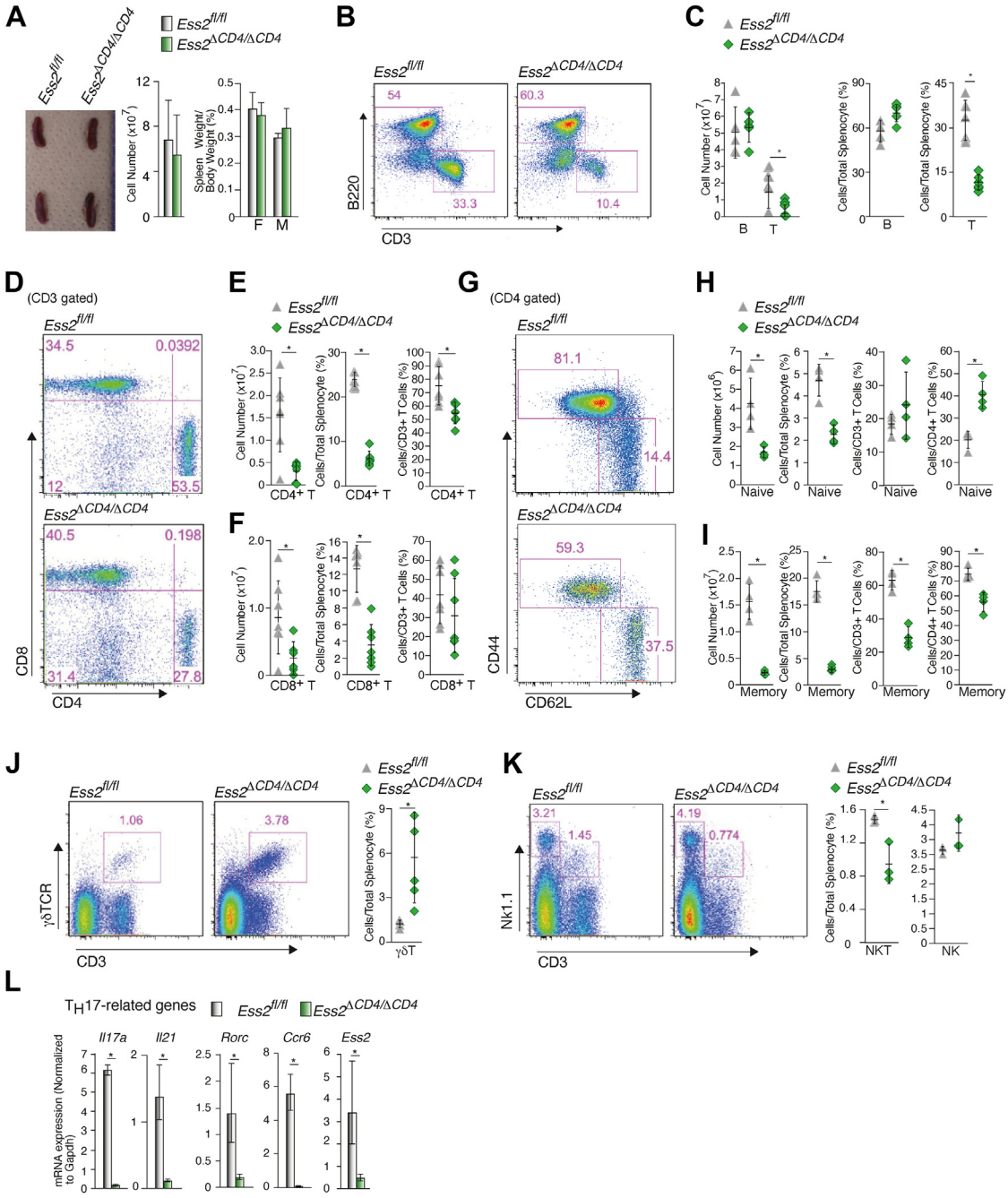

Figure 2. *Ess2*$^{\Delta CD4/\Delta CD4}$ mice show aberrant T-cell development in splenocytes. *A*, representative spleens (*left panel*), quantification of splenocytes (*middle panel*), and spleen weights (*right panel*) in *Ess2*$^{fl/fl}$ and *Ess2*$^{\Delta CD4/\Delta CD4}$ mice. Scale bar = 1 mm. For flow cytometry, the following experiments were carried out under the same conditions: panels *B* and *C*; panels *D–F*; and panels *G–I*. *B*, representative population of B and T cells among the splenocytes of *Ess2*$^{fl/fl}$ and *Ess2*$^{\Delta CD4/\Delta CD4}$ mice as measured by flow cytometry. *C*, quantification of B cells and T cells in *Ess2*$^{fl/fl}$ and *Ess2*$^{\Delta CD4/\Delta CD4}$ mice. *D*, a representative population of CD4$^+$ or CD8$^+$ T cells as assessed by flow cytometry. *E*, quantification of CD4$^+$ T cells in splenocytes and total CD3$^+$ T cells. *F*, quantification of CD8$^+$ T cells in splenocytes and total CD3$^+$ T cells from. *G*, a representative population of naïve and memory CD4$^+$ T cells as assessed by flow cytometry. *H*, quantification of naïve CD4$^+$ T cells in total splenocytes, total CD3$^+$ T cells, and total CD4$^+$ T cells from splenocytes. *I*, quantification of memory CD4$^+$ T cells in total splenocytes, total CD3$^+$ T cells, and total CD4$^+$ T cells from splenocytes. *J*, a representative population of γδT cells as assessed by flow cytometry (*left* and *middle panels*) and the quantification of γδT cells in splenocytes (*right panel*). *K*, a representative population of NKT cells as assessed by flow cytometry (*left* and *middle panels*) and the quantification of NKT cells in splenocytes (*right panel*). *L*, RT-qPCR analysis of primary CD4$^+$ T cells cultured under T_H17 conditions. The mRNA levels of all genes were normalized to the level of *Gapdh* mRNA expression. Each experiment was performed at least three times and the results are presented as the mean ± SD. Each experiment used 3 to 7 mice. *p* values were calculated using Student's *t* test, **p* < 0.05. qPCR, quantitative polymerase chain reaction.

CD4$^+$ T cells to splenocytes and CD8$^+$ T cells to splenocytes were both significantly decreased in *Ess2*$^{\Delta CD4/\Delta CD4}$ mice (Fig. 2, *E* and *F*). The ratio of CD4$^+$ T cells to CD3$^+$ T cells was reduced in *Ess2*$^{\Delta CD4/\Delta CD4}$ mice, whereas the ratio of CD8$^+$ T cells to CD3$^+$ T cells was not significantly different (Fig. 2, *E* and *F*). In addition, the number of naïve CD4$^+$ T cells was only 30% of those in *Ess2*$^{fl/fl}$ mice (Fig. 2, *G* and *H*). While the ratio of naïve CD4$^+$ T cells to total splenocytes was also lower in

Ess2$^{\Delta CD4/\Delta CD4}$ mice, the ratio of naïve CD4$^+$ T cells to total CD4$^+$ T cells was higher, when compared to the *Ess2*$^{fl/fl}$ mice (Fig. 2*H*). However, unlike the naïve cells, the ratio of *Ess2*$^{\Delta CD4/\Delta CD4}$ memory CD4$^+$ T cells to total CD3$^+$ T cells or CD4$^+$ T cells was significantly lower than that of the *Ess2*$^{fl/fl}$ mice (Fig. 2*I*).

Interestingly, *Ess2*$^{\Delta CD4/\Delta CD4}$ mice had significantly more γδT cells and fewer natural killer (NK) T cells than *Ess2*$^{fl/fl}$ mice (Fig. 2, *J* and *K*). There was no significant difference in regulatory T cells (Fig. S2*A*). Next, naïve CD4$^+$ T cells were cultured under T_H17 conditions (Fig. 2*L*). As expected, the mRNA expression levels of T_H17-related genes (*Il17a*, *Il21*, *Rorc*, and *Ccr6*) were lower in the *Ess2*$^{\Delta CD4/\Delta CD4}$ mice. These data suggest that the loss of the Ess2 gene alters T-cell development in the spleen of *Ess2*$^{\Delta CD4/\Delta CD4}$ mice.

Ess2 does not contribute to DN/DP selection in the thymus

Our results indicated that Ess2 regulates naïve T-cell development and/or proliferation. To determine at what stage Ess2 is active in T-cell development, we determined the number of CD4SP and CD8SP thymocytes in the thymuses of *Ess2*$^{fl/fl}$ and *Ess2*$^{\Delta CD4/\Delta CD4}$ mice. *Ess2* mRNA expression levels in DN and CD8SP thymocytes did not differ between *Ess2*$^{fl/fl}$ and *Ess2*$^{\Delta CD4/\Delta CD4}$ mice (Fig. 1*D*). These results suggest that the deletion of *Ess2* in *Ess2*$^{\Delta CD4/\Delta CD4}$ mice occurs during the DP stage. Thymus sizes and weights were similar in both mouse genotypes (Fig. 3*A*). Both positive and negative thymocyte selection occurred normally in *Ess2*$^{\Delta CD4/\Delta CD4}$ mice (Figs. 3, *B* and *C*, and S2*B*). We next determined the expression of two thymocyte regulatory genes (*Ccr7* and *S1pr1*) in CD4SP thymocytes by RT-quantitative PCR (qPCR) (Fig. 3*D*). The *Ccr7* gene product regulates the export of positively selected thymocytes from the thymus (16, 17), and *S1pr1* is highly upregulated in T-cell development to promote the exit of mature T cells from the thymus (18). *Ccr7* and *S1pr1* mRNA expression levels did not differ between *Ess2*$^{\Delta CD4/\Delta CD4}$ and *Ess2*$^{fl/fl}$ mice (Fig. 3*D*). Splenic γδT cells (Fig. 3*E*) also increased, while NKT cells decreased (Fig. 3*F*) in the thymus of *Ess2*$^{\Delta CD4/\Delta CD4}$ mice. These results indicate that Ess2 does not contribute to the positive/negative selection of T cells or their migration from the thymus. However, Ess2 does affect the development of γδT cells and NKT cells in the thymus.

Ess2 regulates mRNA gene expression in CD4SP cells

Our results showed that an *Ess2* deletion in CD4SP thymocytes reduces naïve T-cell numbers; however, the molecular mechanism is poorly understood. To investigate this mechanism, we compared the expression of several CD4$^+$ T-cell-related genes in CD4SP thymocytes and naïve T cells from *Ess2*$^{fl/fl}$ and *Ess2*$^{\Delta CD4/\Delta CD4}$mice; we did not observe any significant differences (Fig. S3).

To elucidate the role of Ess2 in naïve T-cell maintenance, we analyzed the genome-wide RNA expression profiles of DP and CD4SP thymocytes as well as naïve CD4 T-cell splenocytes using RNA-seq (Figs. 4*A* and S4, *A* and *B*). Surprisingly, we observed many Ess2-dependent alterations in mRNA expression in CD4SP thymocytes but only a few in DP thymocytes (Fig. 4, *A* and *B*). Only a few splicing defects were seen in *Ess2*$^{\Delta CD4/\Delta CD4}$ mice (data not shown). Although previous studies show that Ess2 interacts with both the spliceosome and

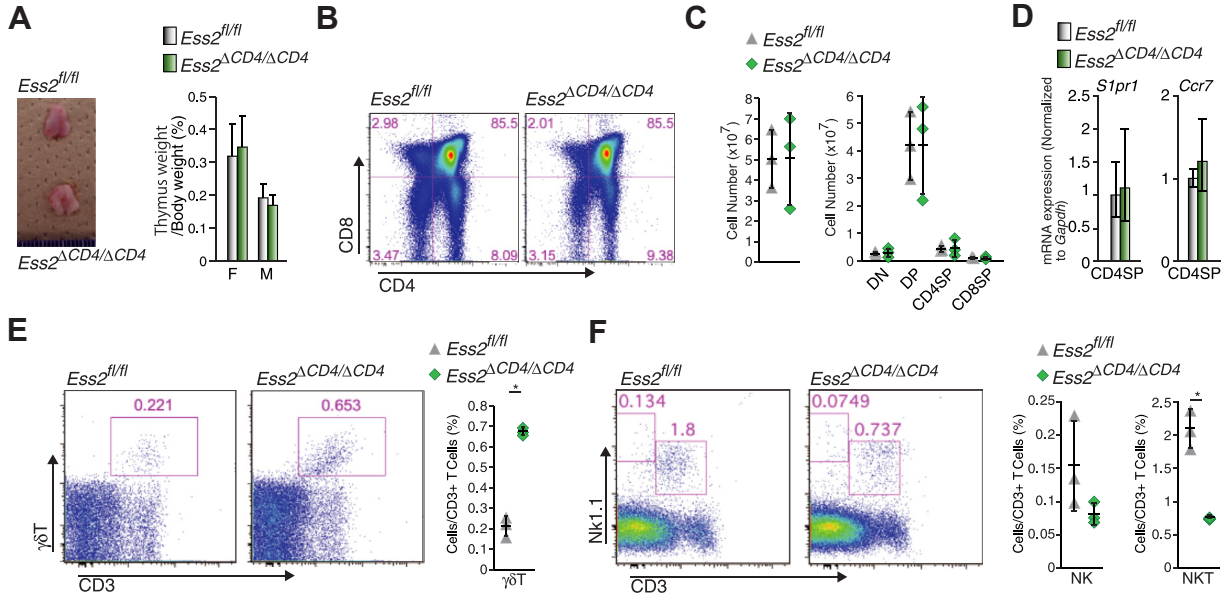

Figure 3. *Ess2*$^{fl/fl}$ and *Ess2*$^{\Delta CD4/\Delta CD4}$ mice exhibit similar numbers of thymocytes. *A*, representative thymus (*left panel*) and thymus weights (*right panel*) of *Ess2*$^{fl/fl}$ and *Ess2*$^{\Delta CD4/\Delta CD4}$. Scale bar = 1 mm. *B*, representative flow cytometry plots of CD4$^-$CD8$^-$ (DN), CD4$^+$CD8$^-$ (CD4P), CD4$^-$CD8$^+$ (CD8SP), and CD4$^+$CD8$^+$ (DP) thymocytes as assessed by flow cytometry. *C*, the whole cell number of thymocytes (*left panel*), DN, CD4SP, CD8SP, and DP cells in *B* (*right panel*). *D*, RT-qPCR of CD4SP-related genes (*S1pr1* and *Ccr7*) in CD4SP cells collected from *Ess2*$^{fl/fl}$ and *Ess2*$^{\Delta CD4/\Delta CD4}$ mice. Three to five mice were used in each experiment. *E*, a representative population of γδT cells as assessed by flow cytometry (*left* and *middle panels*) and the quantification of γδT cells in thymocytes (*right panel*). *F*, a representative population of NKT cells as assessed by flow cytometry (*left* and *middle panels*) and the quantification of NKT cells in thymocytes (*right panel*). Each experiment used three mice. *p* values were calculated using Student's *t* test, *$p < 0.05$. F, female; M, male; qPCR, quantitative polymerase chain reaction.

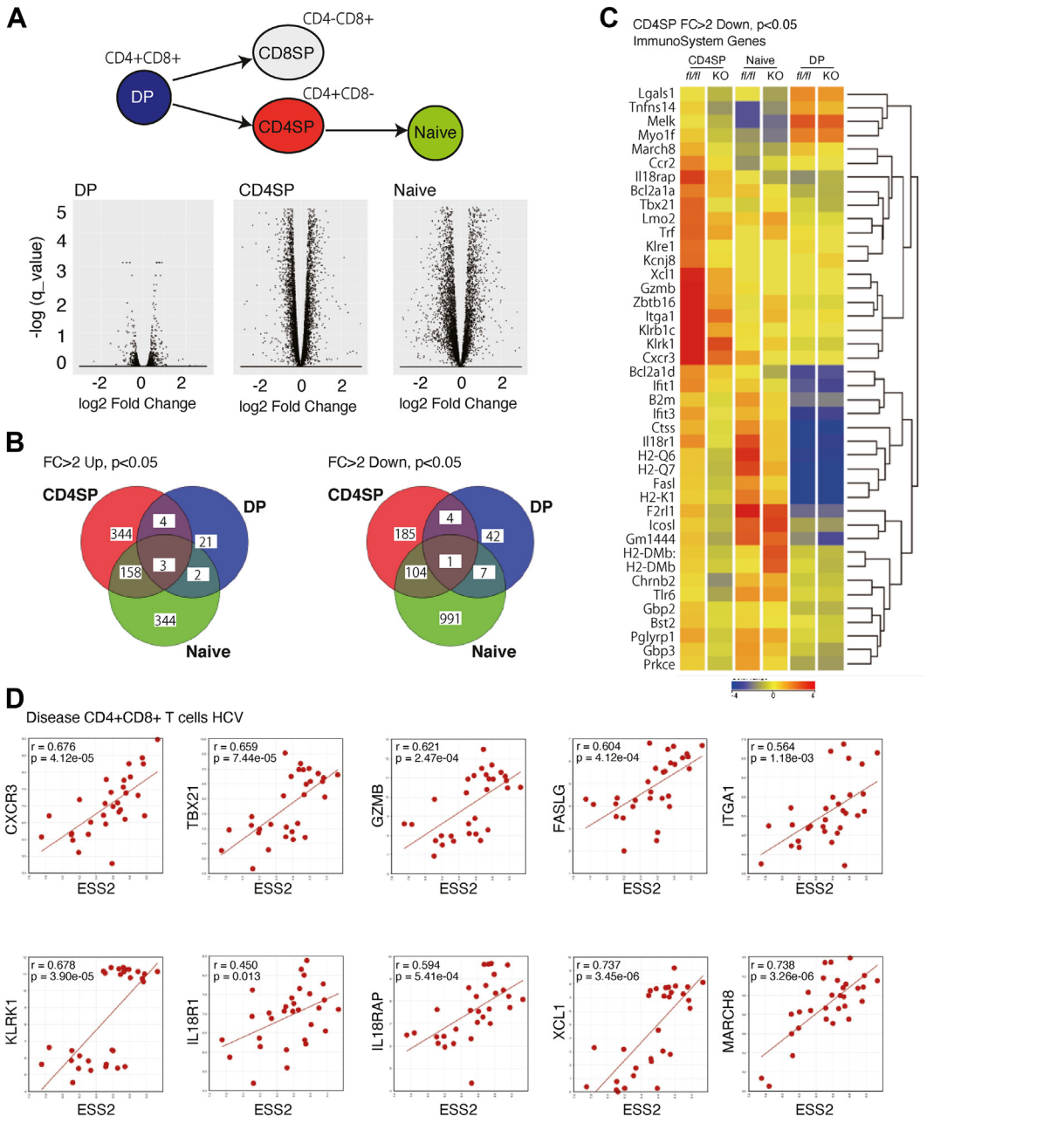

Figure 4. RNA-seq analysis of CD4SP, DP, and naïve T cells from *Ess2*$^{\Delta CD4/\Delta CD4}$ and *Ess2*$^{fl/fl}$ mice. *A*, a volcano plot of CD4SP, DP, and naïve T cells from *Ess2*$^{fl/fl}$ and *Ess2*$^{\Delta CD4/\Delta CD4}$ mice. *B*, a Venn diagram of fold change (FC) in DP thymocytes, CD4SP thymocytes, and naive T cells from *Ess2*$^{fl/fl}$ and *Ess2*$^{\Delta CD4/\Delta CD4}$ mice. *C*, heatmap of immune system genes with a fold change (FC) <2 down in CD4SP thymocytes from *Ess2*$^{fl/fl}$ and *Ess2*$^{\Delta CD4/\Delta CD4}$ mice. The immune system gene set was defined by Strand NGS. *D*, correlation between human ESS2 and some immune system genes in humans using the R2 database (disease CD4+CD8+ T cells HCV).

transcription factors (13), our results indicate that *Ess2* gene deficiency affects transcription starting at the CD4SP stage of development. However, the groups of genes differentially expressed between *Ess2*$^{\Delta CD4/\Delta CD4}$ and *Ess2*$^{fl/fl}$ mice in CD4SP and naïve T cells overlap by only 10 to 30% (Fig. 4*B*). These results suggest that Ess2 regulates different gene sets in CD4SP cells than in naïve T cells.

We confirmed the changes in expression of immune-related genes in CD4SP cells; 42 genes had more than a two-fold difference in expression and some genes were significantly differently expressed in naïve T cells but not DP cells (Fig. 4*C*). To further investigate the clinical significance of *ESS2* expression, we used the R2: Genomics Analysis and Visualization Platform (http://r2.amc.nl). Interestingly, several Ess2-regulated genes were positively correlated with *ESS2* expression in the human disease database of CD4$^+$ and CD8$^+$ T cells isolated from hepatitis C virus patients (19) (GEO source: GSE49954, Fig. 4*D*). These results suggest that they are involved in the ESS2-dependent regulation of the immune system in humans and that *ESS2* expression may be a favorable prognostic factor in autoimmune diseases.

Ess2 regulates Myc target genes

Next, we performed a Database for Annotation, Visualization, and Integrated Discovery (DAVID) pathway analysis and a gene set enrichment analysis (GSEA). The DAVID pathway analysis revealed that genes involved in antigen processing and presentation, cell adhesion, graft-*versus*-host disease, allograft rejection, and type I diabetes mellitus were significantly altered in both $Ess2^{\Delta CD4/\Delta CD4}$ CD4SP thymocytes and naïve T cells compared to $Ess2^{fl/fl}$ cells (Fig. 5*A*). These results show that Ess2 transcriptionally regulates genes from multiple immune pathways.

We next analyzed the HALLMARK gene sets with a GSEA. Both the Myc and oxidative phosphorylation pathways were also altered in $Ess2^{\Delta CD4/\Delta CD4}$ CD4SP thymocytes and naïve T cells (Fig. 5*B*). In $Ess2^{\Delta CD4/\Delta CD4}$ CD4SP thymocytes, IL-2/STAT5-signaling- and allograft-rejection-related gene sets were altered. Other genetic pathways were also changed in $Ess2^{\Delta CD4/\Delta CD4}$ mice (Fig. S6*A* and Table S2). Myc acts as an essential transcription factor in T cells, regulating metabolic reprogramming and proliferation (20). Interestingly, a recent report demonstrated an interaction between Myc and Ess2 through proteomic analysis (21). Based on these observations, we hypothesized that Ess2 acts as a transcriptional co-regulator of Myc. To elucidate the association between Ess2 and Myc, a luciferase reporter assay was performed by over-expressing Ess2 and c-Myc with a luciferase reporter vector (Myc3Elb-Luc) that contained three Myc-binding elements in the HEK293 cell line. As shown in Figure 5*C*, Ess2 enhanced the transcriptional activity of c-Myc in a dose-dependent manner. Additionally, chromatin immunoprecipitation assay (ChIP)-qPCR analysis demonstrated that naïve $CD4^+$ T cells from $Ess2^{\Delta CD4/\Delta CD4}$ mice decrease the recruitment of Ess2 to

A

KEGG_PATHWAY	p-value	
Regulated in CD4SP and Naive	CD4SP	Naive
mmu04612:Antigen processing and presentation	5.26E-05	0.00219
mmu04514:Cell adhesion molecules (CAMs)	0.00025	0.00017
mmu05332:Graft-versus-host disease	0.00533	0.00058
mmu05330:Allograft rejection	0.00875	0.00013
mmu04940:Type I diabetes mellitus	0.00570	0.00400

Regulated in CD4SP	p-value
mmu04512:ECM-receptor interaction	2.09107E-08
mmu04020:Calcium signaling pathway	3.43738E-07
mmu04010:MAPK signaling pathway	2.44515E-05
mmu04151:PI3K-Akt signaling pathway	0.00025
mmu05321:Inflammatory bowel disease (IBD)	0.01224
Regulated in Naive	**p-value**
mmu05323:Rheumatoid arthritis	0.00086
mmu00190:Oxidative phosphorylation	0.00462
mmu05340:Primary immunodeficiency	0.01307
mmu00310:Lysine degradation	0.01400
mmu04144:Endocytosis	0.02554

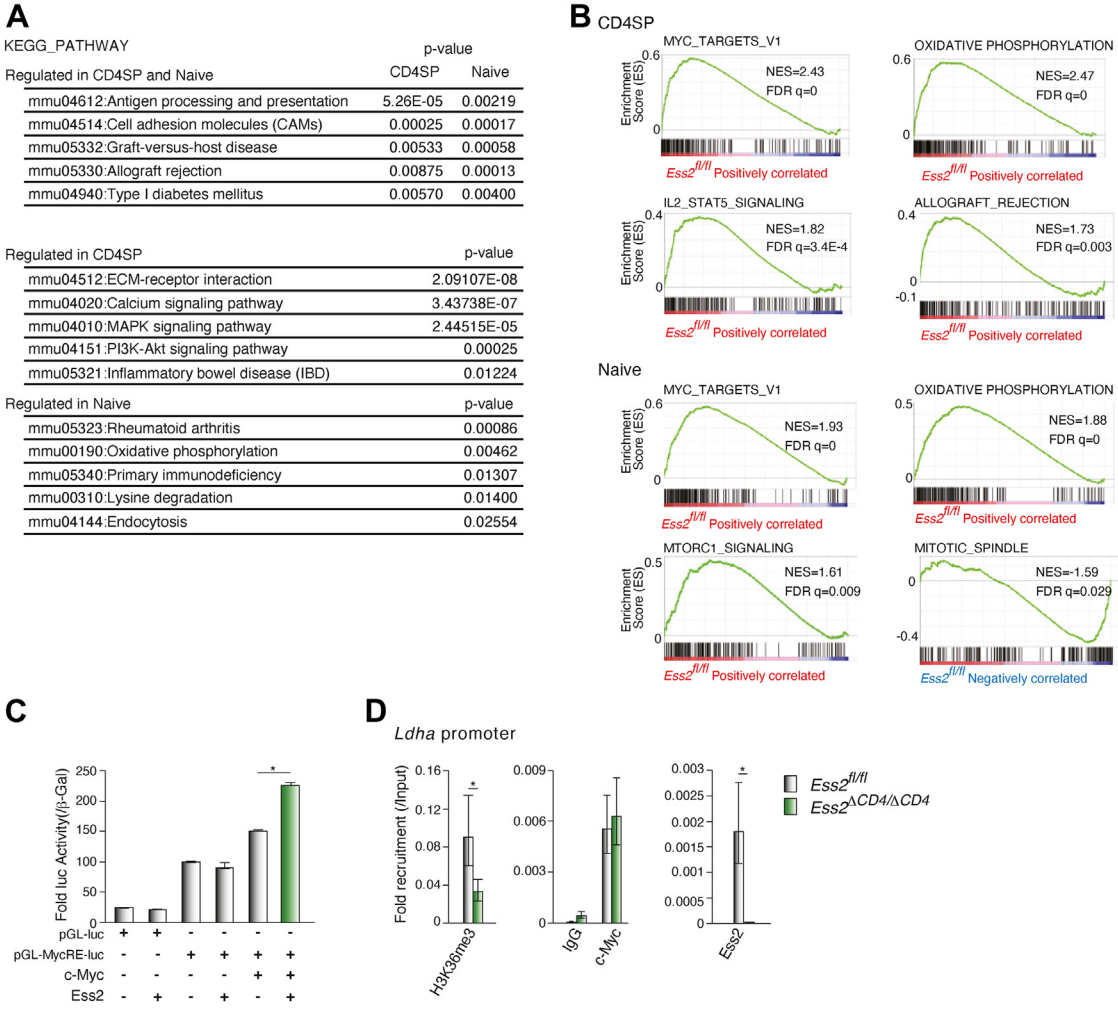

Figure 5. DAVID and GSEA analyses in $Ess2^{fl/fl}$ and $Ess2^{\Delta CD4/\Delta CD4}$ mice. *A*, a DAVID analysis of highly scored gene sets in CD4SP thymocytes or naïve T cells. *B*, representative results of a GSEA analysis in CD4SP and naïve T cells. Among high-scoring gene sets, the immune system–related gene sets were selected (Table S2). *C*, luciferase reporter assay using the luciferase reporter (Myc3Elb-luc), which contains three Myc-binding elements. After transfection of each vector, the HEK293 cells were lysed and a luciferase reporter assay performed. Transcriptional activity was normalized to β-gal activity. *D*, ChIP-qPCR analysis of the *Ldha* promoter using antibodies to Ess2, c-Myc, and histone H3K36me3 in primary naïve $CD4^+$ T cells. Isolated naïve $CD4^+$ T cells were lysed, and the ChIP analyses were performed using the antibodies indicated. qPCR was performed with the primers described in Table S1. Each experiment was performed at least three times, and the results are presented as the mean ± SD. *p* values were calculated using a Student's *t* test, $*p < 0.05$. ChIP, chromatin immunoprecipitation assay; DAVID, Database for Annotation, Visualization, and Integrated Discovery; GSEA, gene set enrichment analysis; qPCR, quantitative polymerase chain reaction.

the *Ldha* promoter, which contains a Myc-binding element (22). Although naïve CD4$^+$ T cells from *Ess2*$^{\Delta CD4/\Delta CD4}$ mice did not alter the recruitment of c-Myc to the *Ldha* promoter (Fig. 5*D*), the levels of the transcriptionally active histone mark, histone H3K36me3, decreased in these cells. Moreover, immunofluorescent staining of overexpressed c-Myc and Ess2-GFP in U2OS cells revealed their co-localization in the nucleus (Fig. S5). These results establish that Ess2 has a direct impact on the transcriptional activity of c-Myc.

ESS2 expression correlates with T-cell-related genes in immune disease patients

Next, we examined the R2 database and found a significant, positive correlation between *ESS2* expression and the T-cell-related genes identified by the GSEA, specifically in lymphocytes of humans infected with hepatitis C virus, Mixed Lymphoma - Eckerle [(23), GEO source: GSE14879], Disease CD4-T and B cells - Lauwerys (GEO source: GSE4588), and mixed Crohn disease [(24), GEO source: GSE9686] (Figs. 6 and S6, *A* and *B*). As expected, *ESS2* expression levels significantly correlated with some of the GSEA-identified genes in human patients. These results show that ESS2 may have similar functions in humans and mice, which is through Myc-targeted gene regulation.

Ess2 regulates IL-7-dependent CD4$^+$ T-cell maintenance

The IL-7 signaling pathway regulates naïve T-cell survival and proliferation (25, 26), and since *IL-7R* mRNA was reduced in CD4SP cells isolated from *Ess2*$^{\Delta CD4/\Delta CD4}$ mice (Figs. 7, *A* and *B* and S4*B*; Table S3), we hypothesized that Ess2 may regulate IL-7-dependent CD4$^+$ T-cell maintenance. ChIP-qPCR analysis showed that deletion of the Ess2 gene decreased the recruitment of the histone H3K36me3 marker to the *Il7r* promoter (Fig. 7*C*). We cultured naïve CD4$^+$ T cells from *Ess2*$^{fl/fl}$ and *Ess2*$^{\Delta CD4/\Delta CD4}$ mice with or without IL-7 for 3 days. As expected, IL-7 maintained the survival of cells isolated from *Ess2*$^{fl/fl}$ but not from *Ess2*$^{\Delta CD4/\Delta CD4}$ (Fig. 7*D*). We observed a similar number of apoptotic *Ess2*$^{\Delta CD4/\Delta CD4}$ naïve CD4$^+$ T cells regardless of the IL-7 treatment (Fig. 7, *E* and *F*). Although IL-2 synergizes with IL-7 to enhance T-cell proliferation, we did not observe alterations in the IL-2-related gene expression of *Ess2*$^{\Delta CD4/\Delta CD4}$ naïve CD4$^+$ T cells (Fig. S3). Next, we examined cell survival, stimulated by anti-CD3ε/CD28 antibodies, with and without IL-7. As shown in Figure 7*G*, *Ess2*$^{\Delta CD4/\Delta CD4}$ naïve CD4$^+$ T cells reduced TCR-activation-

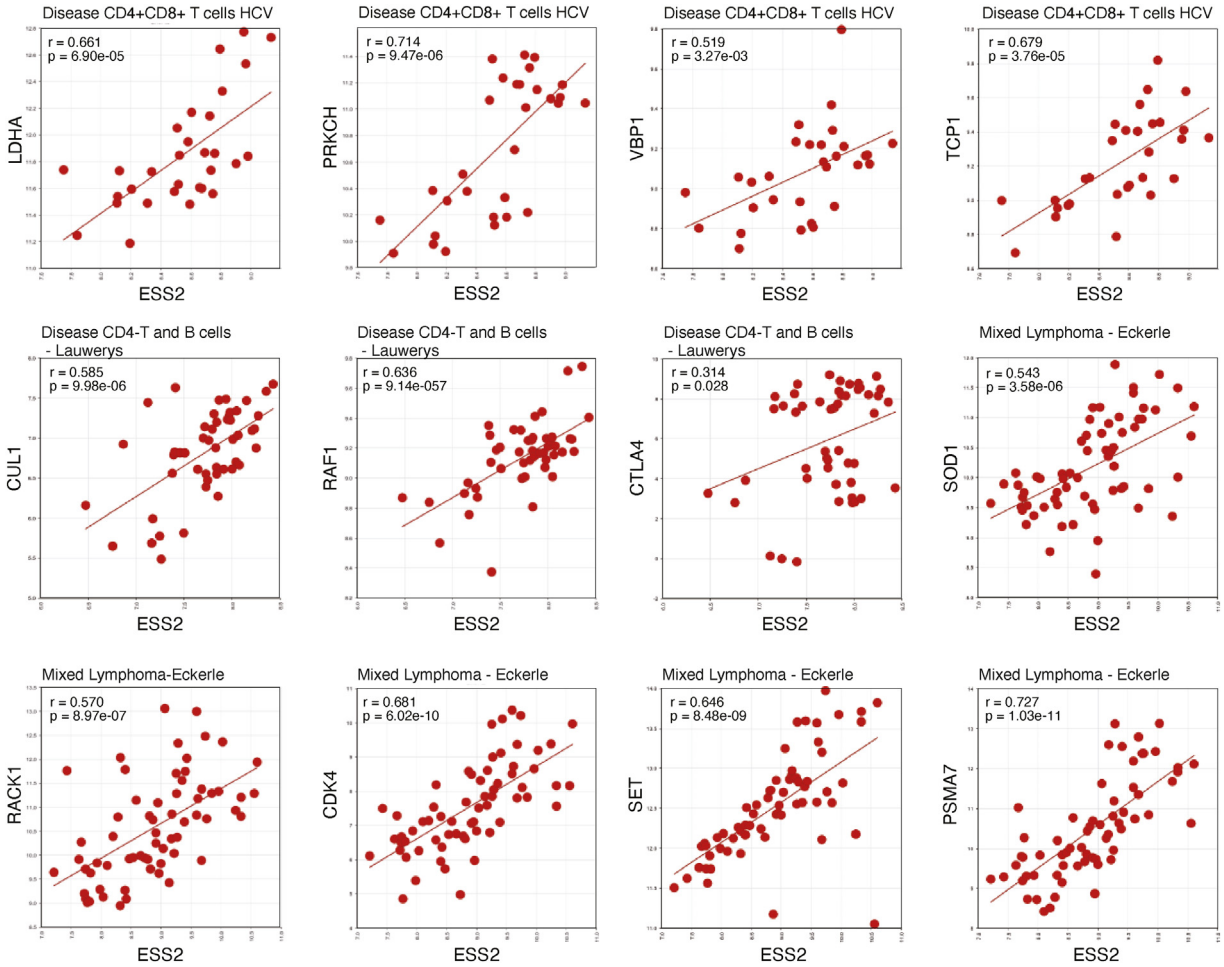

Figure 6. Correlation between human *ESS2* and *Myc* target genes. The correlation between *ESS2* and identified *Myc* target genes in humans using the R2 database. The datasets used are shown in each graph.

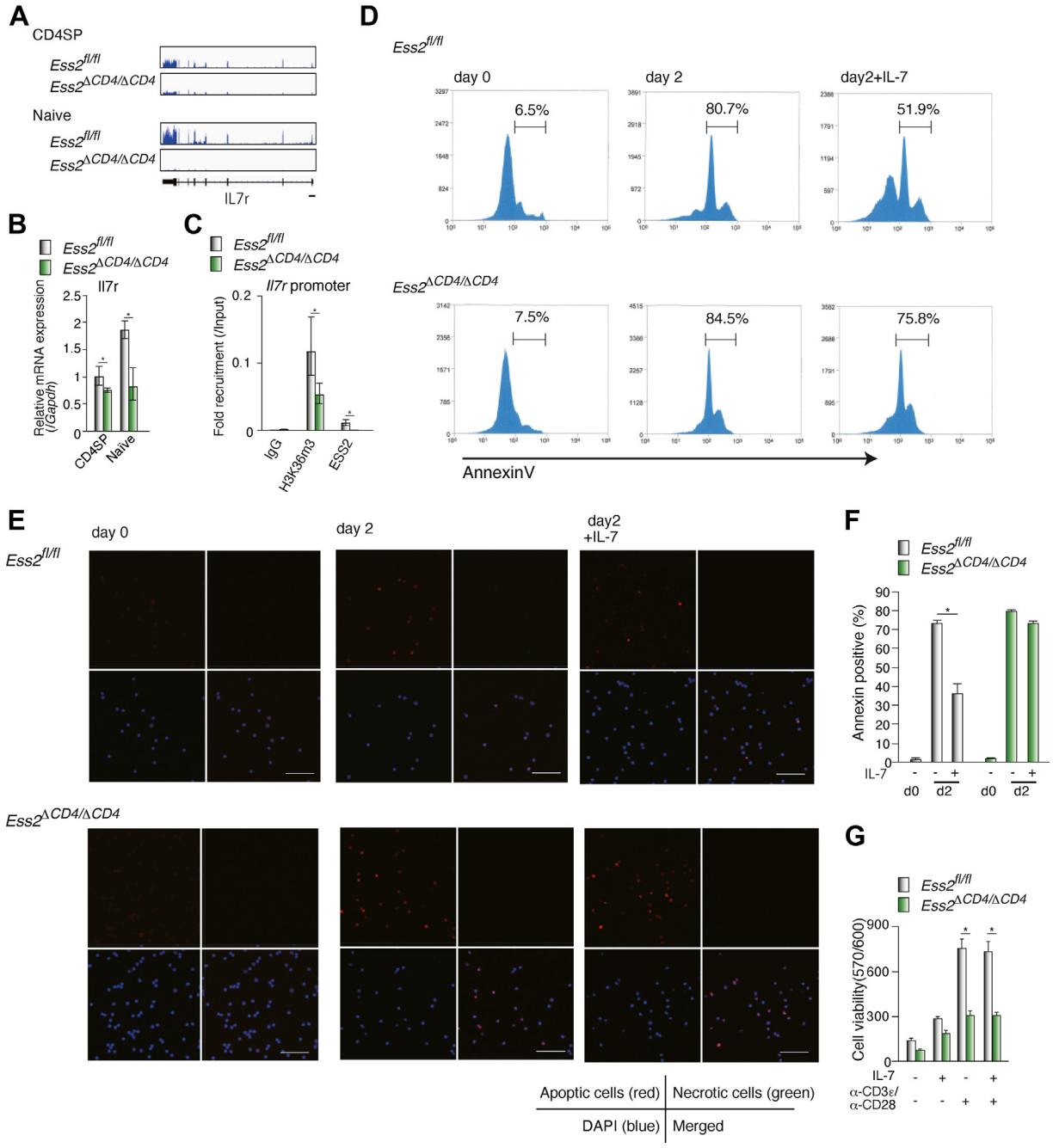

Figure 7. Ess2 regulates IL-7-dependent cell survival in naïve CD4$^+$ T cells. *Ess2$^{fl/fl}$* and *Ess2$^{ΔCD4/ΔCD4}$* naïve T cells were cultured with or without 100 ng ml^{-1} of IL-7. *A*, RNA-seq peaks in the IL7r promoter from CD4SP cells and naïve T cells by IGV. *B*, RT-qPCR of Il7r in CD4SP cells and naïve T cells normalized to the level of *Gapdh* mRNA expression. Three to five mice were used in each experiment, *$p < 0.05$. *C*, ChIP-qPCR analysis of the *Il7r* promoter with anti-Ess2 and anti-histoneH3K36me3 antibodies in primary naïve CD4$^+$ T cells. *D*, representative apoptotic cells stained by Annexin V using flow cytometry (MoFlo XDP). Central and left peaks were Annexin-positive cells, and the percentages are described. *E*, representative confocal microscopy of apoptotic (*red*), necrotic (*green*), and DAPI (*blue*) staining; Scale bar = 50 μm. *F*, quantification of apoptotic cells. The number of cells counted is from 50 to 80. Each sample was counted in at least five areas. *G*, Presto blue staining of naïve CD4$^+$ T cells stimulated with and without anti-CD3ε/CD28 antibodies and/or IL-7 for 2 days. Each experiment was performed at least three times, and the results are presented as the mean ± SD. *p* values were calculated using a Student's *t* test, *$p < 0.05$. ChIP, chromatin immunoprecipitation assay; qPCR, quantitative polymerase chain reaction.

dependent proliferative effects. These results suggest that Ess2 regulates naïve T-cell survival through the IL-7 signaling pathway.

Discussion

In this study, we successfully generated *Ess2$^{fl/fl}$* mice and CD4-specific *Ess2* KO mice for the first time. As previously described (14), we found that *Ess2$^{-/-}$* mice had an early embryonic lethality (Fig. S1*C*). These results indicate that Ess2 plays an essential role in early embryogenesis, although the precise mechanism is unclear.

Unexpectedly, *Ess2$^{ΔCD4/ΔCD4}$* mice produced reduced CD3$^+$ T-cell and NKT-cell numbers but had increased numbers of γδT cells. In *Ess2$^{ΔCD4/ΔCD4}$* mice, the ratio of CD4$^+$ T cells to splenocytes or total CD3$^+$ T cells decreased. Additionally, the ratio

of naïve $CD4^+$ T cells to total $CD4^+$ T cells increased, while the ratio of memory $CD4^+$ T cells to $CD3^+$ T cells or total $CD4^+$ T cells decreased. Such alterations in the ratios of naïve and memory $CD4^+$ T cells in $Ess2^{\Delta CD4/\Delta CD4}$ mice may be due to the different impact that *ESS2* has on cell survival in naïve or memory $CD4^+$ T cells. Further studies will be required in order to characterize this mechanism. Genome-wide RNA expression analyses revealed that Ess2 transcriptionally regulates several genes in thymic CD4SP cells. In particular, the expression of Myc target genes and oxidative phosphorylation pathway genes was decreased significantly in $Ess2^{\Delta CD4/\Delta CD4}$ CD4SP thymocytes and naïve T cells, which may be the cause of reduced naïve T-cell counts in these mice. Interestingly, our findings demonstrated that Ess2 acts as a transcriptional co-regulator for the transcriptional activity of c-Myc and that Ess2 is co-localized with c-Myc in the nucleus. In addition, the expression levels of several Myc target genes, such as *LDHA*, *RACK1*, and *CDK4*, are correlated with *ESS2* expression in immunodeficient patients (Fig. 6). These results suggest that Ess2 controls $CD4^+$ T-cell survival and homeostasis *via* transcriptional regulation through c-Myc and RORγ/γt (Fig. S7). Additional studies may elucidate the detailed mechanism(s) behind Ess2-dependent transcriptional activation. Importantly, our findings show that deletion of *Ess2* caused transcriptional dysfunction, rather than splicing defects. These findings suggest a significant role for Ess2 as a transcriptional co-regulator in the immune system.

Additionally, our findings show that $Ess2^{\Delta CD4/\Delta CD4}$ mice exhibit dysregulation in both γδT and NKT cells. γδT cells develop from DN thymocytes in the thymus, and some transcription factors that regulate γδT-cell development have been identified (27). One such regulator is IL7R; CD4-Cre IL7R deficient mice similarly increased the number of thymic DN and γδT cells (28). Because $Ess2^{\Delta CD4/\Delta CD4}$ naïve T cells exhibited reduced *Il7r* mRNA levels (Fig. 7, *A* and *B*), as well as disrupted IL-7 signal-dependent cell survival (Fig. 7, *D*–*G*), we conclude that Ess2-dependent regulation of the IL-7 signaling pathway may be required to maintain γδT-cell survival. It is unclear, however, whether Ess2 regulates the function of STAT5 and other downstream transcription factors in the IL-7 signaling pathway. Furthermore, there are many transcription factors involved in γδT-cell differentiation (27), and it is unclear which of these are regulated by Ess2. Future studies will focus on elucidating the function of Ess2 in γδT cells.

NKT cells are a heterogeneous subset of T lymphocytes that are developmentally and functionally distinct from conventional $CD4^+$ and $CD8^+$ T cells (29). While T cells and NKT cells both originate in the thymus, their selection requirements are divergent. NKT-cell development occurs in the thymus from a common precursor pool of DP thymocytes and requires several transcription factors, such as NF-κB, GATA3, and RORγt. Because Ess2 localizes to the nucleus and regulates RORγ/γt activity, NKT cells in $Ess2^{\Delta CD4/\Delta CD4}$ mice may reduce RORγ/γt activity in DP thymocytes. Additional studies are required to elucidate the role of Ess2 on the transcriptional regulation of NKT cells.

Interestingly, human *ESS2* expression correlated with the expression of several immune- and oxidative-phosphorylation-related genes in autoimmune disease patients (Figs. 4*D* and 6). These results suggest that Ess2 may also contribute to immunity and metabolism in humans. However, a more detailed analysis is necessary, and a functional analysis of Ess2 in a conditional KO mouse model may help elucidate the molecular mechanism of Ess2-related immune abnormalities. Our previous studies showed that Ess2 induces T_H17 differentiation by enhancing the transcriptional activities of RORγ/γt (2). In $Ess2^{\Delta CD4/\Delta CD4}$ mice, T_H17-related gene mRNA levels were also suppressed in primary $CD4^+$ T cells cultured under T_H17 conditions (Fig. 2*L*). However, in this study, we found that Ess2 affects earlier stages of T-cell maturation which are independent of RORγ/γt. For future studies, additional Cre transgenic mice will be necessary to investigate the function of all T_H cells *in vivo*.

RORγ KO mice regulate naïve T-cell proliferation through Bcl2 expression (30), which did not occur in $Ess2^{\Delta CD4/\Delta CD4}$ mice (data not shown). These results show that the Ess2 protein associates with several transcription factors to regulate their activity, which may also contribute to Ess2-specific immune regulation.

Several mouse models of 22q11DS exist (31), including 22q11.2 deletion heterozygous mice and 22q11DS-associated transgenic mice (32–34). A recent study has reported the generation of a CRISPR-Cas-mediated deletion of 22q11DS (35). Several 22q11DS phenotypes can be analyzed using these mouse models, such as cardiac development, abnormal cranial base morphology, and schizophrenia. However, the causal genes within the 22q11.2 deletion region that are related to immunodeficiency have not yet been reported. We measured the concentration of several cytokines from the blood of $Ess2^{fl/fl}$ and $Ess2^{\Delta CD4/\Delta CD4}$ mice under normal conditions; however, no significant differences were observed (data not shown). Our results suggest that a more detailed analysis of $Ess2^{fl/fl}$ and $Ess2^{\Delta CD4/\Delta CD4}$ mice may provide additional insights into 22q11DS as it regards immunodeficiency.

In summary, we generated both $Ess2^{fl/fl}$ and $Ess2^{\Delta CD4/\Delta CD4}$ mice and have demonstrated a role for Ess2 in post thymic T-cell survival. These findings will enable future work to elucidate the role of Ess2 in the regulation of the immune system.

Experimental procedures

Generation of heterozygous Ess2 ($Ess2^{+/-}$), $Ess2^{fl/f}$, *and* $Ess2^{\Delta CD4/\Delta CD4}$ *mice*

To generate $Ess2^{+/-}$ mice, we purchased the *Ess2* targeting vector (PG00129_Y_4_A10, Wellcome Trust Sanger Institute) from BACPAC Resources Center CHORI (Fig. S1*A*). The targeting vector was linearized and electroporated into RENKA embryonic stem (ES) cell lines derived from the C57BL/6 mouse strain (TransGenic Inc). After screening by genomic southern blot and PCR, *Ess2* gene-targeted ES cells were isolated. Positive ES cell clones were then injected into blastocysts derived from C57BL/6 mice. Successfully injected embryos were transferred into the uteri of pseudopregnant foster mothers and the resulting chimeric mice crossed with C57BL/6 mice. $Ess2^{+/-}$ mice were identified in the F1 generation, demonstrating the germ-line transmission of the *Ess2* mutation. $Ess2^{+/-}$ mice were then backcrossed for five

generations with C57BL/6 background mice to obtain $Ess2^{+/-}$ mice. We generated the $Ess2^{-/-}$ mice by crossing male and female $Ess2^{+/-}$ mice. The heterozygous deletion of *Ess2* was confirmed by genomic southern blotting (Fig. S1*B*).

To generate $Ess2^{fl/fl}$ mice (Fig. S1*A*), $Ess2^{+/-}$ mice were crossed with FLPe transgenic mice [RIKEN, BRC No. 01834_B6-Tg(CAG-FLPe)36 (36)]. $Ess2^{fl/fl}$ mice were then crossed with CD4-Cre transgenic mice (15), and finally male and female $Ess2^{\Delta CD4/+}$ mice were crossed to generate the $Ess2^{\Delta CD4/\Delta CD4}$ mice. $Ess2^{\Delta CD4/\Delta CD4}$ mice were confirmed with genotyping PCR using primer sets #1/#2, #3/#4 (Fig. 1*A* and Table S1), and #1/#4 (Fig. 1*B*).

All mice were raised in specific pathogen-free conditions. Animal experiments were performed according to national and institutional animal care and ethical guidelines and were approved by Nihon University.

Antibodies

For flow cytometry analysis, antibodies specific for CD3e (2C11), CD19 (6D5), CD11b (M1/70), CD11c (N418), CD4 (RM4-5), CD8a (GK1.5 or 53.67), DX5 (DX5), Gr-1 (RBC-8C5), Ter-119 (Ter-119), and CD62L (MEL14) were purchased from BD Biosciences, BioLegend, and eBioscience.

For ChIP-qPCR analysis, an Ess2 specific antibody was generated in our laboratory (13), and an antibody, specific for c-Myc (9402S), was purchased from Cell Signaling Technology.

Flow cytometry

Splenocytes and thymocytes were separated from 8- to 16-week-old mice and subjected to hypotonic red blood cell lysis (150 mM NH_4Cl, 15 mM $NaHCO_3$, and 0.1 mM EDTA) to generate a single-cell suspension. Single-cell suspensions were stained in FACS buffer (0.5% BSA, 2 mM EDTA in PBS) with Fc block containing Zombie red (Biolegend). All data were acquired on a BD LSR Fortessa$_{TM}$ (BD Bioscience) and analyzed using FlowJo software (TreeStar).

RNA isolation and quantitative RT-PCR

Total RNA was extracted using TRIzol (Invitrogen). First-strand cDNA was synthesized from total RNA using PrimeScript Reverse Transcriptase (Takara Bio Inc). For qPCR, an ABI PRISM7000 (Thermo Fisher Scientific) or StepOne (Applied Biosystems) system was used with the Light Cycler SYBR Green I Master Mix (Takara). The relative quantitation value is expressed as $2^{-\Delta Ct}$, where ΔCt is the difference between the mean cycle threshold (Ct) values of triplicates for each sample and that of the *Gapdh* control. Primer sequences were previously described (2) and are listed (Table S1).

RNA-seq and bioinformatics

CD4 single-positive (CD4SP, $CD4^+CD8^-$), double-positive (DP, $CD4^+CD8^+$), and naïve T cells ($CD4^+CD62L^+CD44^-CD25^-$) were sorted with a FACSAria II cell sorter (BD Biosciences), and RNA was extracted with TRIzol (Invitrogen). Single-end RNA-seq was performed using the Illumina HiSeq 2500 (Illumina, Inc). We obtained 101-bp single reads from cDNA fragments. For data analysis, tRNA and rRNA reads were first filtered out using the UCSC Genome Browser. RNA-seq reads were aligned to the mouse genome (mm10 downloaded from Ensembl Genome Browser) using the software TopHat (version 2.0.8 (37)). The raw read counts for each gene were analyzed using the edgeR package.

Gene expression of annotated transcripts was calculated from mapped RNA-seq reads using Cuffdiff to obtain FPKM (fragments per kilobase of exon per million fragments mapped)-normalized gene expression values (38). Some data were normalized and visualized using Strand NGS software (Strand Life Sciences).

To visualize RNA-Seq signals, Bam files were generated and loaded into IGV [Integrative Genomics Viewer, Broad Institute, https://www.broadinstitute.org/igv/ (39)]. *p*-values of gene-list enrichment were calculated using binomial tests using the R software package. All RNA-seq analyses were performed using three biological replicates.

DAVID analysis and GSEA

RNA-seq data were normalized, and gene ontology term and pathway analyses were performed using the DAVID v6.8 (https://david.ncifcrf.gov/). For gene annotation enrichment analysis, gene names were input into the functional annotation-clustering tool in DAVID (40, 41). Functional annotation clustering was performed with the default criteria, and the enrichment score for each annotation cluster was determined. GSEA was performed using the GSEA software package (GSEA v2.2.3), and all gene set files were obtained from the GSEA website (www.broadinstitute.org/gsea/).

Primary naïve T-cell culture

Naïve $CD4^+$ T cells ($CD3^+$, $CD4^+$, $CD62L^{high}$, $CD44^{Nega}$) from spleens were isolated using the Naive $CD4^+$ T-Cell Isolation Kit (Miltenyi Biotec) and cultured in 10% FBS RPMI1640 with or without 100 ng ml^{-1}IL-7. Apoptotic and necrotic cells were identified using Apoptotic and Necrotic Detection Kits (AAT Bioquest Inc) by fluorescence confocal microscopy (LSM710, Carl Zeiss), and apoptotic cells were counted using ImageJ software (NIH). For measuring cell viability, primary cultured naïve T cells were stained with a PrestoBlue Cell Viability Reagent (A13261; Thermo Fisher Scientific) and fluorescence excision was measured at 570 nm and emission 600 nm using the Flex Station 3G (Molecular Devices).

For T_H17 cell differentiation, naïve T cells were cultured under T_H 17 conditions (1 μg ml^{-1} anti-CD3ε, 1 μg ml^{-1} anti-CD28, 1 μg ml^{-1} anti-IL-4, 1 μg ml^{-1} anti-IFN-γ, 10 ng ml^{-1} IL-6 [Peprotech], and 2 ng ml^{-1} TGF-β) for 3 days, and then the RNA was extracted.

Luciferase reporter assays

For the luciferase reporter assays, HEK293 cells were transfected using the Lipofectamine(R) 2000 (Thermo Fisher Scientific) reagent according to the manufacturer's instructions (42). Twenty-four hours after transfection, the cells were harvested and assayed for luciferase and β-galactosidase

activity using a luminometer and a microplate reader (PHERAStar FS, BMG LABTECH). Co-transfection experiments used 150 ng of the reporter plasmid, 10 ng of the pCMX-β-galactosidase expression plasmid, 25 ng of the c-Myc expression plasmid, and 25 ng of the Ess2 expression plasmid for a total 210 ng of the plasmids. Plasmid concentrations were adjusted to equimolar concentrations with the addition of an empty pcDNA3 plasmid for each well in a 96-well plate. Luciferase data were normalized to the internal β-galactosidase control, and all results are presented as the mean ± standard deviation (SD). All transfections were performed in triplicate and repeated at least twice in independent experiments.

ChIP-qPCR analysis

A ChIP was performed according to the manufacturer's instructions (MAGnify ChIP; Thermo Fisher Scientific). Briefly, cells were fixed with 1% formaldehyde (Sigma) and chromatin was sheared by sonication to average lengths between 300 and 500 bp. Chromatin was immunoprecipitated with control IgG or specific antibodies overnight at 4 °C and then incubated with protein A magnetic beads for an additional 2 h. After washing and elution, protein-DNA cross-links were disrupted by heating at 55 °C. Purified DNA was analyzed by qPCR using the StepOne system with SYBR green (Takara Bio). The relative quantitation value was expressed as $2^{-\Delta CT}$, where ΔCT is the difference between the mean CT value, for triplicates of the sample, and that of the input control. The primer sequences used are shown in Table S1.

Statistical analyses

Data are presented as mean ± the SD. Equality of variances was assessed using an F-test. For all statistical analyses, except the RNA-seq analyses, comparisons between two groups were made using a two-tailed Student's *t* test or two-tailed Welch's *t* test, when the variances were equal or unequal, respectively. *p* values less than 0.05 were considered statistically significant. For GSEA, an FDR q-value less than 0.05 was considered statistically significant.

Data availability

The raw data of RNA-seq are publicly available on the GEO repository (Accession No. PRJNA575280). *Ess2*$^{+/-}$ mice (BRC09772) and *Ess2*$^{fl/fl}$ mice (RBRC09771) were registered with the RIKEN BRC. All remaining data are contained within this article and the supporting information.

Supporting information—This article contains supporting information.

Acknowledgments—We thank the members of Prof Makishima's laboratory for helpful discussions and M. Mito (RIKEN) for technical assistance with RNA-seq and southern blotting. We appreciate the Collaborative Research Resources, School of Medicine, Keio University, for technical assistance with our experiments.

Author contributions—I. T. and S. T. conceptualization; I. T., S. H., K. Y., H. O., M. T., and A. Y. methodology; I. T., S. H., S. T., and S. N. data curation; I. T. writing-original draft; S. S. and H. O. software; S. S. and H. O. validation; T. N., T. K., S. N., and M. M. supervision; M. M. writing-review and editing.

Funding and additional information—This study was supported by the Mitsui Life Social Welfare Foundation, Bristol-Myers Squibb, and a Grant-in-Aid for Scientific Research (C; 25462382 and 18K09162).

Conflict of interest—The authors declare that they have no conflicts of interest with the contents of the article.

Abbreviations—The abbreviations used are: ChIP, chromatin immunoprecipitation assay; DAVID, Database for Annotation, Visualization, and Integrated Discovery; DN, double-negative; GSEA, gene set enrichment analysis; KO, knockout; NK, natural killer; qPCR, quantitative polymerase chain reaction.

References

1. Rosenfeld, M. G., Lunyak, V. V., and Glass, C. K. (2006) Sensors and signals: a coactivator/corepressor/epigenetic code for integrating signal-dependent programs of transcriptional response. *Genes Dev.* **20**, 1405–1428
2. Takada, I. (2015) DGCR14 induces Il17a gene expression through the RORgamma/BAZ1B/RSKS2 complex. *Mol. Cell. Biol.* **35**, 344–355
3. Lindsay, E. A., Rizzu, P., Antonacci, R., Jurecic, V., Delmas-Mata, J., Lee, C. C., *et al.* (1996) A transcription map in the CATCH22 critical region: identification, mapping, and ordering of four novel transcripts expressed in heart. *Genomics* **32**, 104–112
4. Rizzu, P., Lindsay, E. A., Taylor, C., O'Donnell, H., Levy, A., Scambler, P., *et al.* (1996) Cloning and comparative mapping of a gene from the commonly deleted region of DiGeorge and Velocardiofacial syndromes conserved in C. elegans. *Mamm. Genome* **7**, 639–643
5. Scambler, P. J. (2000) The 22q11 deletion syndromes. *Hum. Mol. Genet.* **9**, 2421–2426
6. Robin, N. H., and Shprintzen, R. J. (2005) Defining the clinical spectrum of deletion 22q11.2. *J. Pediatr.* **147**, 90–96
7. McDonald-McGinn, D. M., and Sullivan, K. E. (2011) Chromosome 22q11.2 deletion syndrome (DiGeorge syndrome/Velocardiofacial syndrome). *Medicine (Baltimore)* **90**, 1–18
8. Sullivan, K. E. (2019) Chromosome 22q11.2 deletion syndrome and DiGeorge syndrome. *Immunol. Rev.* **287**, 186–201
9. Mangelsdorf, D. J., Thummel, C., Beato, M., Herrlich, P., Schutz, G., Umesono, K., *et al.* (1995) The nuclear receptor superfamily: the second decade. *Cell* **83**, 835–839
10. Jetten, A. M. (2009) Retinoid-related orphan receptors (RORs): critical roles in development, immunity, circadian rhythm, and cellular metabolism. *Nucl. Recept. Signal* **7**, e003
11. Bessonov, S., Anokhina, M., Will, C. L., Urlaub, H., and Luhrmann, R. (2008) Isolation of an active step I spliceosome and composition of its RNP core. *Nature* **452**, 846–850
12. Hegele, A., Kamburov, A., Grossmann, A., Sourlis, C., Wowro, S., Weimann, M., *et al.* (2012) Dynamic protein-protein interaction wiring of the human spliceosome. *Mol. Cell* **45**, 567–580
13. Takada, I., Tsuchiya, M., Yanaka, K., Hidano, S., Takahashi, S., Kobayashi, T., *et al.* (2018) Ess2 bridges transcriptional regulators and spliceosomal complexes via distinct interacting domains. *Biochem. Biophys. Res. Commun.* **497**, 597–604
14. Lindsay, E. A., Botta, A., Jurecic, V., Carattini-Rivera, S., Cheah, Y. C., Rosenblatt, H. M., *et al.* (1999) Congenital heart disease in mice deficient for the DiGeorge syndrome region. *Nature* **401**, 379–383
15. Lee, P. P., Fitzpatrick, D. R., Beard, C., Jessup, H. K., Lehar, S., Makar, K. W., *et al.* (2001) A critical role for Dnmt1 and DNA methylation in T cell development, function, and survival. *Immunity* **15**, 763–774
16. Daley, S. R., Hu, D. Y., and Goodnow, C. C. (2013) Helios marks strongly autoreactive CD4+ T cells in two major waves of thymic deletion

distinguished by induction of PD-1 or NF-kappaB. *J. Exp. Med.* **210**, 269–285
17. Ueno, T., Saito, F., Gray, D. H., Kuse, S., Hieshima, K., Nakano, H., *et al.* (2004) CCR7 signals are essential for cortex-medulla migration of developing thymocytes. *J. Exp. Med.* **200**, 493–505
18. Matloubian, M., Lo, C. G., Cinamon, G., Lesneski, M. J., Xu, Y., Brinkmann, V., *et al.* (2004) Lymphocyte egress from thymus and peripheral lymphoid organs is dependent on S1P receptor 1. *Nature* **427**, 355–360
19. Zhao, B. B., Zheng, S. J., Gong, L. L., Wang, Y., Chen, C. F., Jin, W. J., *et al.* (2013) T lymphocytes from chronic HCV-infected patients are primed for activation-induced apoptosis and express unique pro-apoptotic gene signature. *PLoS One* **8**, e77008
20. Wang, R., Dillon, C. P., Shi, L. Z., Milasta, S., Carter, R., Finkelstein, D., *et al.* (2011) The transcription factor Myc controls metabolic reprogramming upon T lymphocyte activation. *Immunity* **35**, 871–882
21. Kalkat, M., Resetca, D., Lourenco, C., Chan, P. K., Wei, Y., Shiah, Y. J., *et al.* (2018) MYC protein interactome profiling Reveals functionally distinct regions that cooperate to drive tumorigenesis. *Mol. Cell* **72**, 836–848.e7
22. Shim, H., Dolde, C., Lewis, B. C., Wu, C. S., Dang, G., Jungmann, R. A., *et al.* (1997) c-Myc transactivation of LDH-A: implications for tumor metabolism and growth. *Proc. Natl. Acad. Sci. U. S. A.* **94**, 6658–6663
23. Eckerle, S., Brune, V., Doring, C., Tiacci, E., Bohle, V., Sundstrom, C., *et al.* (2009) Gene expression profiling of isolated tumour cells from anaplastic large cell lymphomas: insights into its cellular origin, pathogenesis and relation to Hodgkin lymphoma. *Leukemia* **23**, 2129–2138
24. Carey, R., Jurickova, I., Ballard, E., Bonkowski, E., Han, X., Xu, H., *et al.* (2008) Activation of an IL-6:STAT3-dependent transcriptome in pediatric-onset inflammatory bowel disease. *Inflamm. Bowel Dis.* **14**, 446–457
25. Marrack, P., Bender, J., Hildeman, D., Jordan, M., Mitchell, T., Murakami, M., *et al.* (2000) Homeostasis of alpha beta TCR+ T cells. *Nat. Immunol.* **1**, 107–111
26. Fry, T. J., and Mackall, C. L. (2005) The many faces of IL-7: from lymphopoiesis to peripheral T cell maintenance. *J. Immunol.* **174**, 6571–6576
27. Fiala, G. J., Gomes, A. Q., and Silva-Santos, B. (2020) From thymus to periphery: molecular basis of effector gammadelta-T cell differentiation. *Immunol. Rev.* **298**, 47–60
28. Tani-ichi, S., Shimba, A., Wagatsuma, K., Miyachi, H., Kitano, S., Imai, K., *et al.* (2013) Interleukin-7 receptor controls development and maturation of late stages of thymocyte subpopulations. *Proc. Natl. Acad. Sci. U. S. A.* **110**, 612–617
29. Das, R., Sant'Angelo, D. B., and Nichols, K. E. (2010) Transcriptional control of invariant NKT cell development. *Immunol. Rev.* **238**, 195–215
30. Sun, Z., Unutmaz, D., Zou, Y. R., Sunshine, M. J., Pierani, A., Brenner-Morton, S., *et al.* (2000) Requirement for RORgamma in thymocyte survival and lymphoid organ development. *Science* **288**, 2369–2373
31. Guna, A., Butcher, N. J., and Bassett, A. S. (2015) Comparative mapping of the 22q11.2 deletion region and the potential of simple model organisms. *J. Neurodev. Disord.* **7**, 18
32. Meechan, D. W., Maynard, T. M., Tucker, E. S., Fernandez, A., Karpinski, B. A., Rothblat, L. A., *et al.* (2015) Modeling a model: mouse genetics, 22q11.2 deletion syndrome, and disorders of cortical circuit development. *Prog. Neurobiol.* **130**, 1–28
33. Sumitomo, A., Horike, K., Hirai, K., Butcher, N., Boot, E., Sakurai, T., *et al.* (2018) A mouse model of 22q11.2 deletions: molecular and behavioral signatures of Parkinson's disease and schizophrenia. *Sci. Adv.* **4**, eaar6637
34. Motahari, Z., Moody, S. A., Maynard, T. M., and LaMantia, A. S. (2019) In the line-up: deleted genes associated with DiGeorge/22q11.2 deletion syndrome: are they all suspects? *J. Neurodev. Disord.* **11**, 7
35. Saito, R., Koebis, M., Nagai, T., Shimizu, K., Liao, J., Wulaer, B., *et al.* (2020) Comprehensive analysis of a novel mouse model of the 22q11.2 deletion syndrome: a model with the most common 3.0-Mb deletion at the human 22q11.2 locus. *Transl. Psychiatry* **10**, 35
36. Kanki, H., Suzuki, H., and Itohara, S. (2006) High-efficiency CAG-FLPe deleter mice in C57BL/6J background. *Exp. Anim.* **55**, 137–141
37. Kim, D., and Salzberg, S. L. (2011) TopHat-fusion: an algorithm for discovery of novel fusion transcripts. *Genome Biol.* **12**, R72
38. Trapnell, C., Roberts, A., Goff, L., Pertea, G., Kim, D., Kelley, D. R., *et al.* (2012) Differential gene and transcript expression analysis of RNA-seq experiments with TopHat and Cufflinks. *Nat. Protoc.* **7**, 562–578
39. Robinson, J. T., Thorvaldsdottir, H., Winckler, W., Guttman, M., Lander, E. S., Getz, G., *et al.* (2011) Integrative genomics viewer. *Nat. Biotechnol.* **29**, 24–26
40. Huang da, W., Sherman, B. T., and Lempicki, R. A. (2009) Systematic and integrative analysis of large gene lists using DAVID bioinformatics resources. *Nat. Protoc.* **4**, 44–57
41. Huang da, W., Sherman, B. T., and Lempicki, R. A. (2009) Bioinformatics enrichment tools: paths toward the comprehensive functional analysis of large gene lists. *Nucleic Acids Res.* **37**, 1–13
42. Parvin, R., Noro, E., Saito-Hakoda, A., Shimada, H., Suzuki, S., Shimizu, K., *et al.* (2018) Inhibitory effects of a novel PPAR-gamma agonist MEKT1 on pomc expression/ACTH secretion in AtT20 cells. *PPAR Res.* **2018**, 5346272